

Heterogeneous & Homogeneous & Bio- & Nano-

CHEMCATCHEM

CATALYSIS

Accepted Article

Title: Unraveling Oxygen Reduction Sites in Graphitic Carbon Co-N-C type Electrocatalysts Prepared from Single Precursor Pyrolysis

Authors: Alex Schechter

This manuscript has been accepted after peer review and appears as an Accepted Article online prior to editing, proofing, and formal publication of the final Version of Record (VoR). This work is currently citable by using the Digital Object Identifier (DOI) given below. The VoR will be published online in Early View as soon as possible and may be different to this Accepted Article as a result of editing. Readers should obtain the VoR from the journal website shown below when it is published to ensure accuracy of information. The authors are responsible for the content of this Accepted Article.

To be cited as: *ChemCatChem* 10.1002/cctc.201700324

Link to VoR: <http://dx.doi.org/10.1002/cctc.201700324>

WILEY-VCH

www.chemcatchem.org



Unraveling Oxygen Reduction Sites in Graphitic Carbon Co-N-C type Electrocatalysts Prepared from Single Precursor Pyrolysis

Palaniappan Subramanian, Roopathy Mohan and Alex Schechter*

Department of Chemical Sciences, Ariel University, Ariel 40700, Israel

Abstract:

Metal and nitrogen doped carbon based hybrid materials (M-N-C) are widely regarded as promising alternative to platinum for catalyzing oxygen reduction reaction in fuel cell cathodes. Two important steps involved in the preparation of these catalysts are acid wash and reheat treatment of the pyrolyzed mixture made of carbon (C), nitrogen (N) and metal precursors (M). We have explored in detail the changes induced by the post-treatment steps on structure, composition and oxygen reduction activity of new hybrid catalysts prepared by prolonged pyrolysis of single well defined organometallic precursor. The marginal increase in nitrogen content, apparent BET surface area, porosity, surface defects, and higher degree of graphitization have positively contributed to the substantial improvement in ORR activity of post treated catalysts in alkaline solution, whereas this procedure is found to have weaker influence on ORR activity in acid solution. The findings from this study suggest that both free and nitrogen coordinated metal, specifically 'Co₂N' sites present in the catalyst bulk protected by nitrogen doped graphitic carbon layer is most likely the active site in 'Co-N-C' catalysts. Based on these experimental results, we have proposed a model that will assist in improving the understanding of plausible functioning of these active sites in acid and alkaline solution.

Keywords: cobalt phthalocyanine; acid wash; second heat treatment; oxygen reduction reaction; M-N-C catalyst.

*Corresponding authors. *Tel:* +972-3-9371470; *fax:* +972-3-9076586.
E-mail address: salex@ariel.ac.il

1. Introduction

Exploring materials to find a suitable alternative for replacing Pt in fuel cell cathodes is an ongoing effort made by scientists and it has only intensified in the past decade ^[1]. Extensive studies were done on pyrolysis of macrocycles with a metal-nitrogen (M-N₄) function ^[2] after the discovery of cobalt phthalocyanine as active oxygen reduction catalyst ^[3]. Recently, it was found that active oxygen reduction catalysts prepared from pyrolysis of precursor mixtures composed of metal (Fe and/or Co), nitrogen and carbon without pre-existing M-N₄ function has spectroscopically identifiable uncoordinated metal and nitrogen centers ^[4]. On the other hand, investigative studies carried out on a different Fe-N-C based oxygen reduction catalysts active in acidic solution point towards the presence of bifunctional centers namely Fe-N/C and Fe nanoparticles/C post heat treatment at high temperature ^[5]. A. Zitolo *et. al.* have identified the presence of two FeN₄ porphyrinic structures with different O₂ adsorption modes using extensive analysis of XANES data ^[6].

Several approaches have emerged in terms of materials synthesis and wide variety of metal-nitrogen-carbon (M-N-C) precursors and pyrolysis conditions have been reported to yield oxygen reduction catalyst active either in acid or alkaline solutions ^[7]. These include but are not limited to using nitrogen containing polymer based molecules such as polyaniline and polyethyleneimine, employing metal chelating agents such as 1,10-phenanthroline^[8], pyridine^[9], ethylenediaminetetraacetic ^[10], using templates such as metal organic framework ^[11] or silica ^[12] ZnO ^[13] particles to produce high surface area nitrogen doped mesoporous graphitic carbons. One of the pioneering study in recent times is reported by Zelenay *et. al.* on the formation of most active and durable non-Pt catalyst obtained by pyrolysis of polyaniline, iron and/or cobalt ^[14]. In this report, the authors have employed an acid washing step (post-treatment of the first heat treated

catalyst with 0.5 M H₂SO₄ for 8 h) followed by a second heat treatment step (900°C for 3 h under nitrogen atmosphere). We have prepared a composite catalysts with new phases - previously unreported by prolonged pyrolysis of unsupported cobalt phthalocyanine (CoPc) molecule. The above-said post treatment steps improved the oxygen reduction activity of the catalyst manifold and hence explored in detail the structural and compositional changes induced by these two steps in the newly prepared composite catalysts.

Some recent studies suggest that metal based sites are not necessary for electrochemical oxygen reduction reaction, especially in alkaline solutions ^[15]. On the other hand, a number of other reports, unequivocally point toward the critical importance of metal-nitrogen coordinated sites M-N_x (in most cases M = Fe) in acid solution ORR ^[5, 16]. These sites are essentially embedded within the microporous skeleton of the carbon scaffold of non-PGM catalysts ^[8], when the metal center is coordinated with pyridinic ^[17] or pyrrolic ^[18] nitrogen atoms. The contrasting reports in literature show that there is still no clarity on the role of metal centers in M-N-C type non-platinum group metal catalysts and it mostly depends on the synthetic strategy adopted for preparing the catalysts.

It should be emphasized that CoPc is a well-studied molecule in the field of oxygen reduction electrocatalysis. There are also few reports published recently on Co_x-N containing hybrid catalysts prepared using CoPc as an organometallic precursor ^[19]. These catalysts are composed of Co_x-N core and nitrogen doped graphitic carbon shell whereas the catalysts reported herein is made of Co₂N structures in the bulk covered by nitrogen doped graphitic carbon sheets. Further, we have explained the difference in activity seen in acid and alkaline solution based on the structures evolved after post treatment. The activity differences noticed in this Co-N-C type catalysts is not explored in any of the reports cited above. We are of the view that unraveling the chemical functions evolved subsequent to post treating carbonized CoPc will help us better understand the

factors responsible for the enhanced ORR activity observed in the post treated catalysts. Henceforth we describe in detail in the following sections the specific changes noticed in the physicochemical properties of unsupported cobalt phthalocyanine molecule subjected to prolonged pyrolysis and post treatment steps and their distinct effect on ORR activity in alkaline and acid solutions.

2. Experimental Section

2.1. Preparation of carbonized cobalt phthalocyanine

The synthesis of carbonized cobalt phthalocyanine, herein termed as ‘Co-N-C-1’ was carried out by the thermal decomposition of cobalt phthalocyanine (CoPc) [97%, purum, Sigma-Aldrich]. Co-N-C-1 was synthesized by heat treating 0.1 g CoPc in an open ceramic vessel under N₂ (99.999% pure) flow (0.5 l/min). The temperature was raised to 900°C with a ramp rate of 5°C per minute and maintained at the same temperature for 6 h. After cooling by natural convection (~6 h) of the vessel to room temperature, the obtained pyrolyzed sample (black powder) was ground using an agate mortar to obtain a fine powder. The acid washed sample (termed as ‘Co-N-C-1-AW’) and second heat treated sample (herein referred as ‘Co-N-C-2’) was prepared by the following procedure. Co-N-C-1 was dispersed in 0.5 M H₂SO₄ and subsequently stirred at 80°C for 8 h. This acid treated sample was washed several times with water and ethanol until all the acidic residues has been removed followed by drying under vacuum at room temperature. The acid treated sample was further subjected to heat treatment at 900°C under N₂ (99.999% pure) flow (0.5 l/min) for 3 h that yielded a fine and fluffy black powder. The influence of pyrolysis temperature has been reported in our previous publication. Based on the results reported earlier in our paper^[20], we have chosen to study only the sample pyrolysed at 900°C since we intended to explore the origin of

oxygen reduction activity exhibited by the most active catalyst. The carbonized materials were characterized by structural, compositional, morphological, and electrochemical measurements.

2.2. Physicochemical characterizations

Powder X-ray diffraction (XRD) patterns of the samples were measured using a PAnalytical XRD-6000 X-ray diffractometer using Cu K α radiation ($k = 1.5406 \text{ \AA}$) at $4^\circ/\text{min}$. The size and surface morphology of Co-N-C samples were characterized using scanning electron microscopy (SEM; JEOL, Helios 600) operating at 5 keV. The preparation of SEM samples involves the application and spreading of fine powder samples on the surface of the copper tape. The transmission electron microscopy (TEM) was obtained on a JEOL, JEM-1400 using an accelerating voltage of 200 kV. The instrument is equipped with an energy-dispersive X-ray spectroscopy (EDX) accessory. The composition of the obtained materials was characterized by EDX analysis. High Resolution Transmission Electron Microscopic images and the corresponding selected area electron diffraction (SAED) patterns were collected from HRTEM, JEOL JEM-2100 equipped with a LaB₆ emitter operated at 200 kV. Samples for TEM/HRTEM measurements were prepared by making a suspension of the particles in isopropanol, using water-bath sonication. Samples for TEM/HRTEM measurements were prepared by making a suspension of the particles in isopropanol, using water-bath sonication. Two small droplets were then applied on a TEM copper grid, coated with a carbon film and dried under ambient conditions in a covered Petri dish before sample processing. Nitrogen adsorption/desorption isotherms were measured at AAP gold instruments (China) to obtain the Brunauer-Emmett-Teller (BET) surface area. Raman spectra were recorded with a XploRA ONE™ micro-Raman system (Horiba Scientific, France) using 532 nm laser, power <150 mW and spectral data spacing of 1 cm^{-1} . Ex-situ XPS analysis was performed

in a Kratos AXIS-HS spectrometer, using a monochromatized Al K α source. All XPS measurements were carried out at room temperature, under vacuum of 1.0-3.0 x 10⁻⁹ Torr.

2.3. Electrochemical characterizations

Electrochemical experiments were conducted at room temperature on a CHI 760C bipotentiostat (CH Instrument, Texas, USA). A rotating disk electrode (RDE) with a 5 mm diameter glassy carbon (GC) disk (Pine Instruments) served as working electrode; platinum wire and Ag/AgCl electrode were used as counter and reference electrode, respectively. The Co-N-C modified GC working electrode was fabricated by applying 5-10 μ l of catalyst ink followed by drying at room temperature. Typically, Co-N-C catalyst ink was prepared by dispersing 5 mg of Co-N-C-1 or Co-N-C-2 in 0.63 ml of isopropanol/water mixture followed by the addition of 4.16 μ l of 0.5 wt. % Nafion® in isopropanol solution (ion power). The catalyst loading in 2.5 μ l of this catalyst slurry is 0.1 mg cm⁻². The rotating ring disk electrode (RRDE) experiments for studying ORR kinetics were performed over the potential range of 0.1 to 1.2 V vs. RHE at a scan rate of 5 mV s⁻¹ in O₂-saturated 0.1 M KOH or 0.5 M H₂SO₄ solutions. Catalyst poisoning experiments were performed by addition of 10 mM Na₂S to 0.1 M KOH and the catalyst coated electrode is immersed in this solution for 20 minutes after which polarisation measurements were done both in N₂ and O₂ saturated conditions. Pure O₂ - 99.99% and N₂- 99.999% were used in the electrochemical measurements, where applicable.

3. Results and Discussion

3.1. Microscopic and Spectroscopic Characterization:

Scanning Electron Microscopy (SEM) and Transmission Electron Microscopy (TEM) images of Co-N-C-1 and Co-N-C-2 is shown in Figure 1 and 2. The morphological features of Co-N-C-1

(Figure 1a, b and 2a) clearly show the presence of cobalt particles both on the carbon surface and embedded within the carbon layers. It is evident from the microscopic images of Co-N-C-2 (Figure 1c,d and 2b) that most of these cobalt particles present on the surface have been removed by acid treatment carried out on Co-N-C-1. This observation is further substantiated by very small amount of cobalt in Co-N-C-2, surface compositional data obtained from XPS analysis (Table 1) and representative EDX spectral data (Figure 2), cobalt concentration obtained from XRF analysis (Table S1). Further, heat treatment of Co-N-C-1 has induced a change in the morphology of carbon observed as smoother surface composed of relatively thin stacks of transparent carbon layers. HRTEM imaging was performed on Co-N-C-2 to visualize physical bonding state of cobalt particles trapped in between the graphitic carbon layer. Figure. 3a and b displays the HRTEM images and Selected Area Electron Diffraction (SAED) pattern of Co-N-C-2, respectively. Since the cobalt particles were very small in size (≥ 2 nm) and covered by the carbon layers it is difficult to clearly visualize these particles in the microscopic images. However SAED pattern, EDX measurements performed on different regions of the sample consistently indicated the presence of Co, Co₂N particles and graphitic carbon - inferred from matching lattice planes namely (220), (021) and (002), respectively.

The phase composition and structure of Co-N-C catalysts was determined by X-ray diffraction (XRD) studies. Figure 4 provides the XRD pattern of Co-N-C-1 and Co-N-C-2. Powder XRD patterns of Co-N-C-1 depicted in Figure 4a shows the presence of peak at about 26° assigned to the (002) facet of hexagonal graphite (JCPDS file no.34-0567) which illustrates the successful formation of graphitic structure during pyrolysis. Note that the intensity of this peak has increased manifold in Co-N-C-2 (Figure 4b). This observation is indicative of the formation of large number of graphitic structures subsequent to acid washing and second heat treatment steps. The peaks

located at 44.5° , 51.8° and 75.9° appear due to the presence of a single face-centered cubic (fcc) crystalline α -Co phase (JCPDS file no. 15-0806). The three peaks assigned earlier is more prominent in Co-N-C-1 (Figure 4a) than Co-N-C-2 (Figure 4b) and hence the former sample must contain larger number of crystalline cobalt particles. In addition to these features, Co-N-C-2 has peaks at 38.2° and 43.1° attributed to the Co_2N structure (JCPDS File No: 72-1368) that must have formed during second heat treatment done at 900°C in nitrogen atmosphere. We attribute the formation of Co_2N to remains of 'Co' in the carbon bulk, which were not accessible to the acid treatment, and diffused to the particle surface upon exposure to nitrogen during the second heat treatment. This is confirmed by the presence of Co phases appearing in the XRD pattern of Co-N-C-1-AW (Figure S1). Attempts to measure the ^1H and ^{13}C NMR by solid-state probe failed due to strong magnetization of this sample, assigned to magnetic metallic cobalt particles. Hence, in support of carbon protected catalyst particles, similar process expressing the formation of other metals nitrides in N-M-C catalysts seems very likely [16b, 21].

The Raman spectra of Co-N-Cs (Figure 5) display peaks around 1310 cm^{-1} (D band) and 1520 cm^{-1} (G band) as the main peaks. The former is attributed to the hybridized vibration mode associated with defects in graphitic carbon nanostructures, while the latter is assigned to the vibration originating from sp^2 carbon atoms present in the carbonized sample [22]. The intensity ratio of D and G bands ($I_{\text{D}}/I_{\text{G}}$) is a figure of merit used to estimate the defect density in carbon nanostructures. The almost identical $I_{\text{D}}/I_{\text{G}}$ of Co-N-C-1 (1.2) and Co-N-C-2 (1.3) points to the similar amount of defects in heat-treated samples. Plausibly, such defects induced by the N heteroatom and coordinated cobalt ions can aid in the improvement of catalytic performance of Co-N-C catalysts [23]. It is noteworthy to mention that $I_{\text{D}}/I_{\text{G}}$ is only 0.85 in case of acid washed sample (Figure S2) possibly due to reduction of the defects formed during first heat treatment. In addition

to the 'D' and 'G' bands, a peak around 660 cm^{-1} present in Co-N-C-1 and Co-N-C-2 is the Raman-active mode of CoO particles and are close to the value reported in the literature^[24]. This band is less intense in Co-N-C-1-AW (see Figure S2) due to lower amount of Co doping post acid washing. The bands around 1460 and 2680 cm^{-1} in Co-N-C catalysts are seen on account of the two-phonon modes in graphitic carbon^[25]. The apparent Brauner-Emmett-Teller surface (BET) areas of Co-N-C-1 and Co-N-C-2 were found to be 168 and $189\text{ m}^2\text{ g}^{-1}$, respectively (see N_2 adsorption-desorption plot presented in Figure 6a). Pore size distribution for Co-N-C-1 and Co-N-C-2 shown in Figure 6b reveals a narrow distribution of pore sizes in the region of 3.1 - 4.2 nm in both samples. However, there are relatively larger number of small mesopores in Co-N-C-2 also directly attributable to the subjection of catalysts to second heat treatment. The presence of large number of mesopores and narrow pore-size distribution observed in Co-N-C-2 allows better access of the reactants (oxygen and ions) and thus may have a positive influence on the electrochemical activity of these samples towards ORR.

X-ray photoelectron spectroscopy (XPS) was used to investigate the evolution of chemical bonds of N, Co and C induced by pyrolysis and post treatment steps. Figure 7 shows high resolution core level N_{1s} and Co_{2p} X-ray photoelectron spectra of Co-N-C-1 and Co-N-C-2. C, N, Co and O (in case of Co-N-C-1) and C, N, O (in case of Co-N-C-2) elements have been detected (Table 1). The deconvoluted N_{1s} spectra of Co-N-C-1 and Co-N-C-2 shows the presence of pyridinic, pyrrolic, graphitic and oxidized type of nitrogen. N_{1s} spectra of Co-N-C-1-AW (Figure S3) also indicates the presence of all the above-mentioned type of nitrogen species. Figure 7A (b) indicates the presence of relatively large number of graphitic nitrogen in Co-N-C-2 than Co-N-C-1, directly attributable to second heat treatment. $\text{Co}_{2p_{1/2}}$ and $\text{Co}_{2p_{3/2}}$ bands are centered at 779.7 eV and 796.2 eV in Co-N-C-1 with a separation of 15.6 eV between them, typical of Co_3O_4 and consistent with

well-characterized Co_3O_4 reported in the literature [26]. The XPS shows the presence of surface oxidized Co in the form of Co_3O_4 in Co-N-C-1 and Co-N-C-2, XRD which is a bulk structural tool does not have the sensitivity to detect these phases at this low concentrations. There is no detectable Co in Co-N-C-1-AW (Table 1). The Co_{2p} core-level shows shake-up satellite peaks and cobalt species in different oxidation states (Figure 7B). This finding is in line with the high surface oxygen concentration in this sample (Table 1). It can also be seen from Table 1 that there is a marginal increase in surface nitrogen content and N/C ratio in Co-N-C-2 probably due to the interaction of formed ammonia during the second heat treatment performed under nitrogen leading to the modification of the outer surface of carbon particles [27]. Strikingly the shoulder appearing in $\text{Co}_{2p_{3/2}}$ spectra of Co-N-C-2 (Figure 7B.b) attributable to Co-N function is absent in Co-N-C-1. This observation corroborates with the XRD data showing the presence of Co_2N phases only in Co-N-C-2.

3.2. Electrochemical oxygen reduction activity of Co-N-C-1 and Co-N-C-2 catalyst

The ORR activity of Co-N-C-1 and Co-N-C-2 was initially evaluated by cyclic voltammetry (CV) experiments (Figure 8a,b). Cyclic voltammogram of Co-N-C-1 (Figure 8a) in N_2 -saturated 0.1 M KOH shows a redox transition at 1.1 V indicative of Co_3O_4 phase on the surface as determined by XRD, XPS and Raman data. A relatively smaller oxidation peak observed above 1 V in the CV of Co-N-C-2 is possibly due to the removal of most of the surface cobalt/cobalt oxide during acid treatment step. When the electrolyte is saturated with O_2 , a pronounced oxygen reduction wave with $E_{1/2}$ at 0.88 V (Co-N-C-2) is observed. However there are two reduction waves observed in Co-N-C-1 at 0.82 V and 0.55 V. The former is due to oxygen reduction and the latter is attributed to the redox transition of Co_3O_4 .

To gain further insight into ORR activity and reaction kinetics of the Co-N-C catalysts, steady-state polarization measurements were carried out for each of the catalytic electrode in O₂-saturated 0.1 M KOH solution. As shown in Figure 9a and b, the onset potential of ORR in Co-N-C-1 and Co-N-C-2 are 0.9 V and 1.05 V vs. RHE, respectively. The positive shift in the onset potential by 0.105 V and distinct appearance of mass-transport limited current indicates the formation of catalytic sites that improves the oxygen reduction kinetics in alkaline solution. However, it is pertinent to note that despite the removal of cobalt species during acid washing step, it has positive potential shift (lower over potentials) and higher ORR activity. The inference from this experimental observation is that the presence of large amount of metal/metal oxide particles alone will not necessarily result in the enhancement of ORR activity. This is not true when referring to acid solution as there is no dramatic change in activity post acid leaching and second heat treatment (Figure 10 and 11).

Figure 9a and b also shows the comparison of the ORR properties of Co-N-Cs with that of commercial Johnson Matthey 20% Pt/C catalyst in 0.1 M KOH at 1200 rpm. The ORR onset potential of Co-N-C-2 catalysts is 8 mV lower than state of art Pt/C catalyst with a loading of 50 $\mu\text{g}_{\text{Pt}} \text{cm}^{-2}$. Further, the limiting current density is clearly visible only in Co-N-C-2 suggesting that the mass transfer is facilitated in this catalysts due to the faster reduction of O₂ on larger number of active sites dispersed over high surface area and narrow pore size distribution of this catalyst, as well as faster kinetics. This observation is in accordance with the high I_D/I_G ratio obtained from Raman spectroscopy and the presence of Co₂N phases in the catalyst bulk covered by nitrogen doped graphitic carbon structures in Co-N-C-2 as revealed by the XRD and XPS data.

The H₂O₂ oxidation detected by the Pt ring poised at 1.2 V vs. RHE, is plotted as a function of the disk potential in Figure 9d. It is lower than the total ORR current (Figure 9c) indicates that most

of the ORR proceeds via the $4e^-$ pathway. Ring current rises with the overall oxygen reduction current at 0.95 V and increases with the electrode rotation rate, suggesting that H_2O_2 formation is potential dependent. Generation of H_2O_2 is dominant in the low overpotential region of 0.9-0.6 V. At potentials below 0.6 V the rate of peroxide formation remains stable.

The kinetic parameters that serve as an indicator for the reaction pathway are the number of electrons (n) in the overall reaction and the complementary partial O_2 reduction product defined by % H_2O_2 parameter. These parameters were calculated from equations. 1 and 2 using the RRDE results.

$$n = 4I_D / (I_D + I_R/N) \quad (1)$$

$$\%H_2O_2 = 100(2I_R/N) / (I_D + I_R/N) \quad (2)$$

Where 'N' is the collection coefficient of the RRDE electrode whose value is 0.256 (supplied by the manufacturer of RRDE electrode).

The value of diffusion current j_D at a given potential was used to find the kinetic current through the equation 3 given below:

$$1/j_D = 1/j_k + 1/0.62nFC_{O_2}D_{O_2}^{2/3}v^{-1/6}\omega^{1/2}A \quad (3)$$

where j_k is the electrode potential dependent kinetic current density of the ORR, n is the average number of electrons transferred in the overall process of reducing oxygen (the theoretical maximum is 4), F is the Faraday's constant ($96,487 \text{ C mol}^{-1}$), C_{O_2} is the concentration of molecular oxygen in the electrolyte ($1.117 \times 10^{-6} \text{ mol mL}^{-1}$), D_{O_2} is the O_2 diffusion coefficient in aqueous

media ($1.9 \times 10^{-5} \text{ cm}^2 \text{ s}^{-1}$), and ν is the kinetic viscosity of the electrolyte ($0.01073 \text{ cm}^2 \text{ s}^{-1}$ for alkaline solution), ω is the angular velocity in rad s^{-1} , and A is the sectional area of the electrode.

The highest % H_2O_2 formation in Co-N-C-2 is 12.5% at 0.6 V, while the lowest is 4.4% at 0.9 V. At lower potentials of 0.4 V, the % H_2O_2 values of Co-N-C-2 catalyst marginally decrease to 11.7%. These relatively high values of % H_2O_2 are attributed to the presence of few oxidized metal species hindering efficient charge transfer. The number of electrons involved in ORR of Co-N-C-2 is 3.4 at 0.6 V (refer Figure S4 showing the KL plot). This is consistent with the presence of $4e^-$ selective Co containing sites post acid washing and second heat treatment steps.

The Tafel slope calculation was used to analyze the ORR as catalyzed by Co-N-C-2. The calculated Tafel slopes ($\partial\eta/\partial \log I_k$) obtained from currents measured using Co-N-C-2 catalysts in the 120 mV overpotential region - 50 to 125 mV is 55 mV/decade (Figure S5 a) and that in 130-200 mV is 112 mV/decade (Figure S5b). These values suggest that the first step involving oxygen adsorption is slow whereas the reduction of hydrogen peroxide intermediate is relatively faster. This behavior is different from Pt/C where the smaller Tafel slope in the low over potential region corresponds to the ORR at the Oxide covered Pt, and the large slope in the high potential region corresponds to that of a metallic Pt surface [28]. When all the kinetic parameters of the ORR are considered, a two-step process may be actively involved in Co-N-C-2 where oxygen is reduced, mostly to peroxide at low over potentials and subsequent reduction to water in a faster step at higher over potential in a total $2e^- + 2e^-$ mechanism.

The oxygen reduction activity at identical loading ($100 \mu\text{g}/\text{cm}^2$) in acid solution is poor as shown in Figure 10b and 11a and significantly weaker than the activity exhibited by Co-N-C-2 catalyst in alkaline solution (Figure 11c). However, when the loading is increased to $400 \mu\text{g}/\text{cm}^2$ there is

an increase in oxygen reduction current and upshift in onset potential by 130 mV (Figure 11b) possibly due to the relative increase in the number of metallic Co sites. The observed activity in acid solution is correlated with the presence of Co, Co₂N, Co₂O₃ active sites. However, these materials are thermodynamically unstable in acid solution and indeed are present only in small amounts in the surface of these catalysts after the acid treatment step as shown in the XPS and EDX results. Nevertheless, XRD pattern confirms their presence in the bulk of the carbonized particles. Therefore it is highly likely that these active sites are protected by graphitic/graphene sheets formed during the second heat treatment which are seen in the XRD (Figure 4). In [29] it was shown that consecutive heat treatment of carbonized NMC depicts higher graphitic structure as well as increase in the ORR currents. It is worth-mentioning that graphite coating is commonly used in protection of metal surfaces from corrosion [30]. The electrochemical behavior of these protected sites is limited kinetically by the accessibility of O₂ reflected by the high overpotential, the absence of limiting current (Figure 11 a,b) despite increased catalyst loading.

Catalytic poisoning experiments were done by addition of 10 mM Na₂S to 0.1 M KOH under O₂ saturated condition. HS⁻ ions strongly bond to transition metals through the empty d orbitals, thus, block O₂ adsorption to the active sites. The corresponding LSVs recorded on Co-N-C-2 presented in Figure S6 shows the disappearance of oxygen reduction activity, due to the poisoning of active metal sites. These results point to the fact that the metal based sites are the primary oxygen reduction sites in Co-N-C-2 catalysts.

3.3. Insights on the factors governing the oxygen reduction activity of Co-N-C catalysts:

It is important to dissect the role of acid and heat treatment steps separately in order to understand the factors contributing to the enhancement of oxygen reduction activity noticed after carrying out

these procedures. The acid treatment is known to induce the following changes on the catalyst materials. They are (i) removal of unstable cobalt particles present on the surface of Co-N-C-1, (ii) exfoliation of the graphitic carbon layers - inferred from the 2 times increase in capacitive current when compared with 'water washed' sample (control sample prepared by washing with doubled distilled water instead of acid employing identical heat treatment conditions) in acidic as well as alkaline solutions. The second heat treatment carried out under nitrogen atmosphere helps in (i) formation of Co₂N phase in the catalyst upon reaction of the trapped cobalt particles inside the nitrogen doped carbon layers, (ii) formation of nitrogen doped graphitic carbon sheets that helps in improving electronic and ionic conductivity but most importantly facilitates O₂ transport to the protected site to greater extent in alkaline solution and to a lesser extent in acidic solution (iii) possible formation of defects on the surface of carbon due to the drilling effect induced by the removal of cobalt and subsequent heat treatment step, recently explored in detail by G.Zhong et al. [31]. It is also pertinent to note that the second heat treatment done without acid washing step did not lead to any improvement in the oxygen reduction activity both in acidic and alkaline solutions possibly due to the presence of cobalt/cobalt oxide particles on nitrogen doped carbon surfaces hindering the formation of Co₂N based active sites. This observation highlights the critical role of acid washing step before the second heat treatment step. Based on the above experimental observations, we have attempted to explain the oxygen reduction activity differences observed in acidic and alkaline solution. The presence of metallic cobalt, cobalt oxide particles and Co₂N encapsulated by graphitic nitrogen doped carbon layers, defects sites in carbon sheets facilitating oxygen transport to the cobalt based active sites are found to be important factors contributing to the appreciable oxygen reduction activity of Co-N-C-2 in alkaline solutions. In acid solutions, Co-N-C-2 shows only marginal decrease in the onset potential, small increase in the oxygen reduction

current density and restricted mass-transport limited currents when compared with Co-N-C-1. All these can be attributed to the hindered oxygen transport to the encapsulated nitrogen coordinated cobalt sites. The N1s XPS of Co-N-C-2 mixed with acidic polymer indicates a clear shift of 2.1 eV from original pyridinic nitrogen binding energy due to protonation of nitrogen (Figure 12A). This observation is consistent with the recently published article on protonation of pyridinic nitrogen^[32]. On basis of the XPS result, the pyridinic N of Co-N-C-2-Nafion® mixture, it is only logical to claim that Co-N-C-2 should also be protonated in 0.5 M H₂SO₄ solution, leading to change in the charge density (or basicity) of adjacent carbon atoms. Consequently affinity to O₂ is greatly reduced and thus overall ORR activity suffers. Henceforth lower ORR activity in acidic medium than in alkaline medium is attributed to the protonation of pyridinic N. As illustrated in Figure 12B, it is not difficult to understand the restricted oxygen transport in acid solution, when considering the protonation of nitrogen dopants in the graphitic carbon sheets and in alkaline solution they are free to interact with O₂ via nonbonding electrons (e.g. amines).

4. Conclusions

In summary, prolonged pyrolysis and post treatment of unsupported cobalt phthalocyanine yielded a composite catalysts with multiple metallic Co phase compositions. Importantly, the second heat treatment is found to induce the formation of highly graphitized structure of carbon, Co₂N phase and in addition lead to the increased doping of nitrogen. All these changes are found to positively influence the oxygen reduction activity in alkaline solution. However, these structural changes tend to have weaker influence on the ORR activity of these catalysts in acid solution due to restricted oxygen transport to the cobalt based active sites possibly due to the protonation of nitrogen groups. Catalyst poisoning study carried out on graphitic carbon Co-N-C catalysts revealed that metallic cobalt containing sites as the primary active sites for ORR in alkaline

solution. The comparison of activity between acid and alkaline solution revealed the functioning of metallic 'Co' based primary active sites and thus opens the door for exploring active sites and their functioning in M-N-C type catalysts.

Acknowledgements

A.S would like to thank the Israel Science Foundation (ISF) for funding the research work through Israel National Research Center for Electrochemical Propulsion (INREP) and I-CORE Program (number 2797/11). P.S and R.M acknowledges the support of INREP and Ariel University for financial support.

Accepted Manuscript

Table 1 Surface composition (atomic %) of Co-N-C catalysts obtained from XPS

Sample	C/%	O/%	N/%	Co/%	N/C
Co-N-C-1	87.18	9.80	0.65	2.37	0.74
Co-N-C-AW	93.02	6.37	0.61	*	0.65
Co-N-C-2	96.76	1.44	0.90	0.91	0.93

*Below detection limit.

Accepted Manuscript

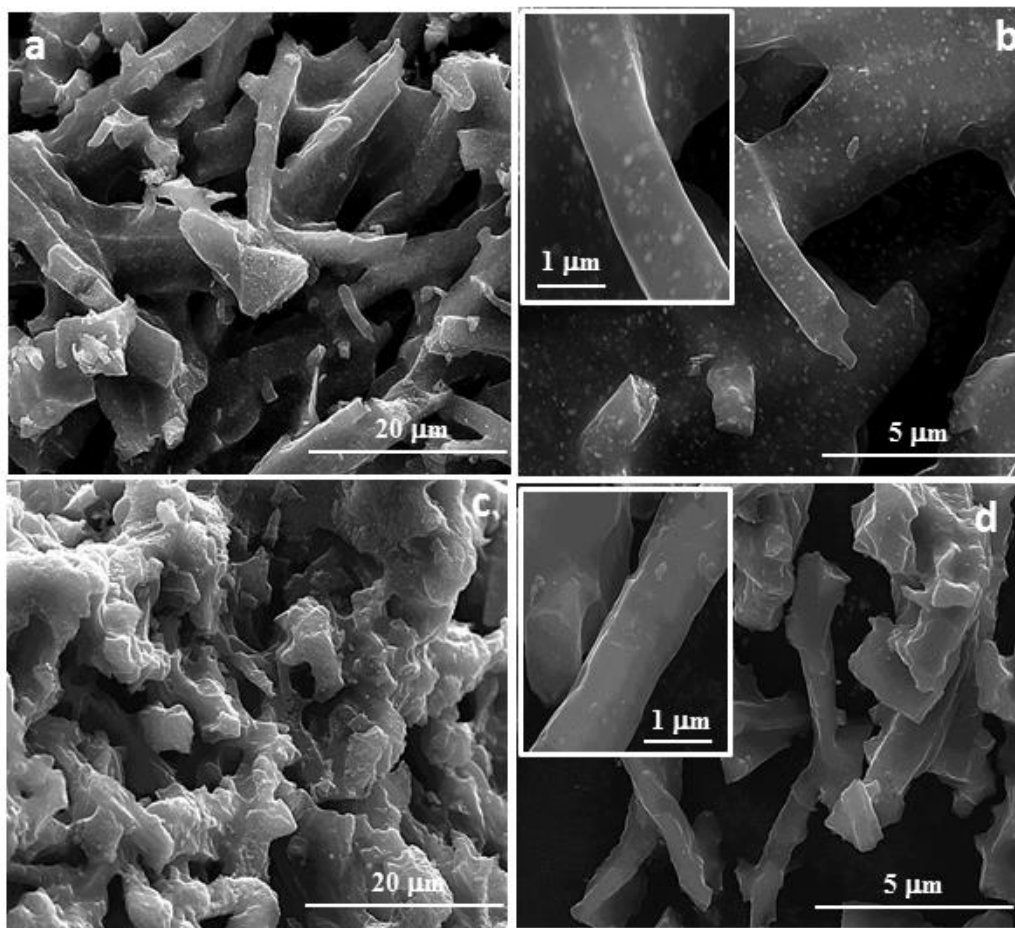


Figure 1 SEM image of Co-N-C-1 - x5000 (low) (a) and x20000 (high) magnification (b); Co-N-C-2 - x5000 (low) (c) and x20000 (high) magnification (d); Inset: Magnified area of a spot selected from 'b' and 'd', respectively.

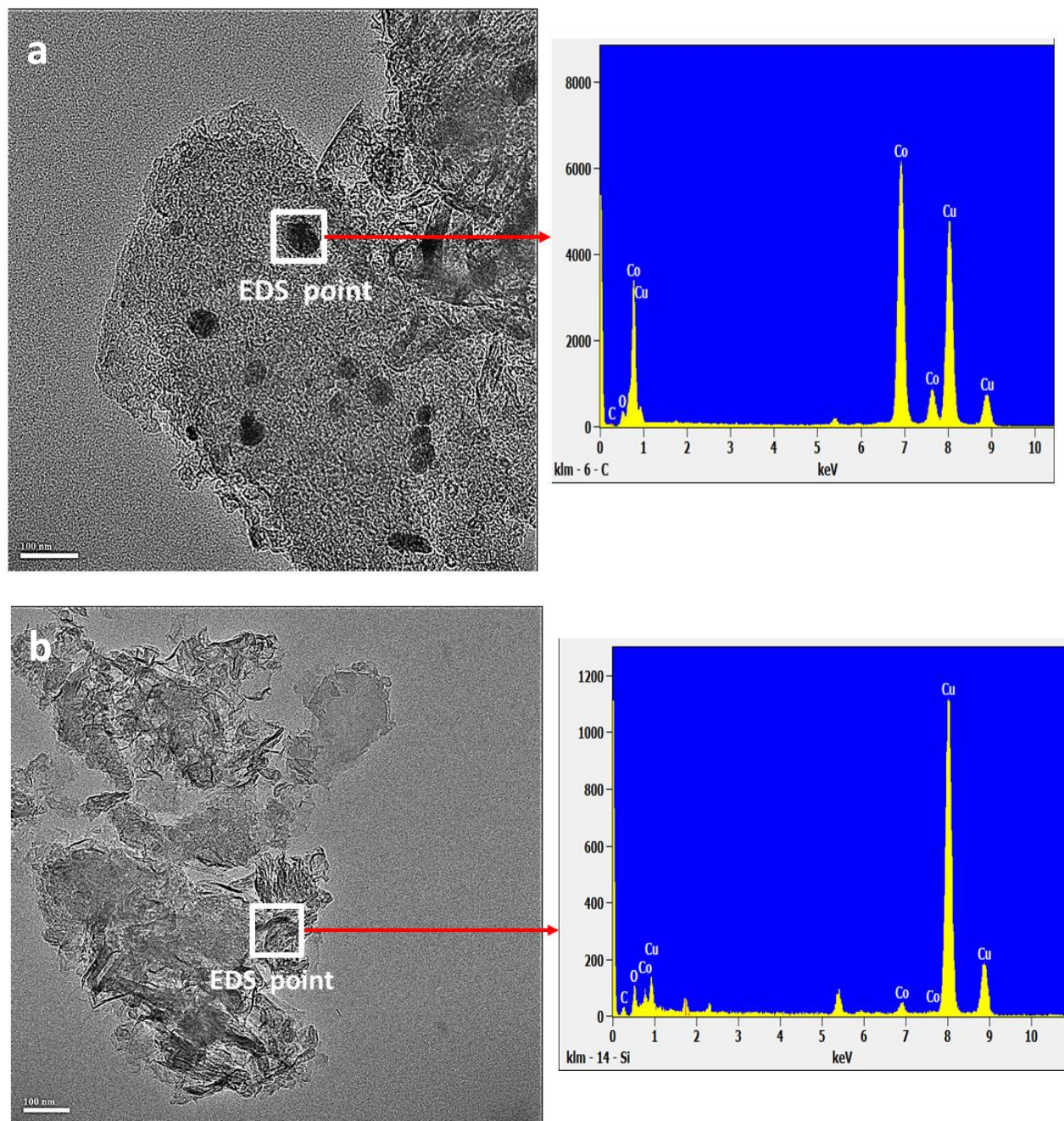


Figure 2 TEM images and corresponding EDX spectrograph of Co-N-C-1 (a), Co-N-C-2 (b). The white square in the TEM picture is the spot where Energy Dispersive X-ray Spectroscopic measurements were made.

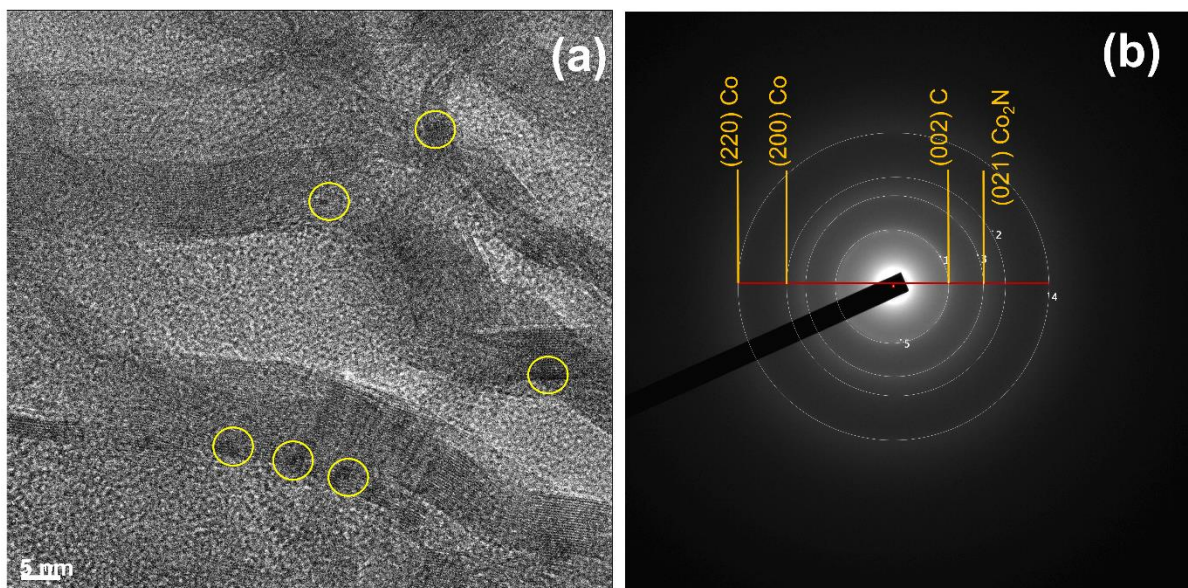


Figure 3 HRTEM image and SAED pattern of Co-N-C-2 (b). The spot marker by yellow circles indicate the both bonded and unbonded cobalt nanoparticles embedded within the carbon layers.

Scale Bar: 5 nm

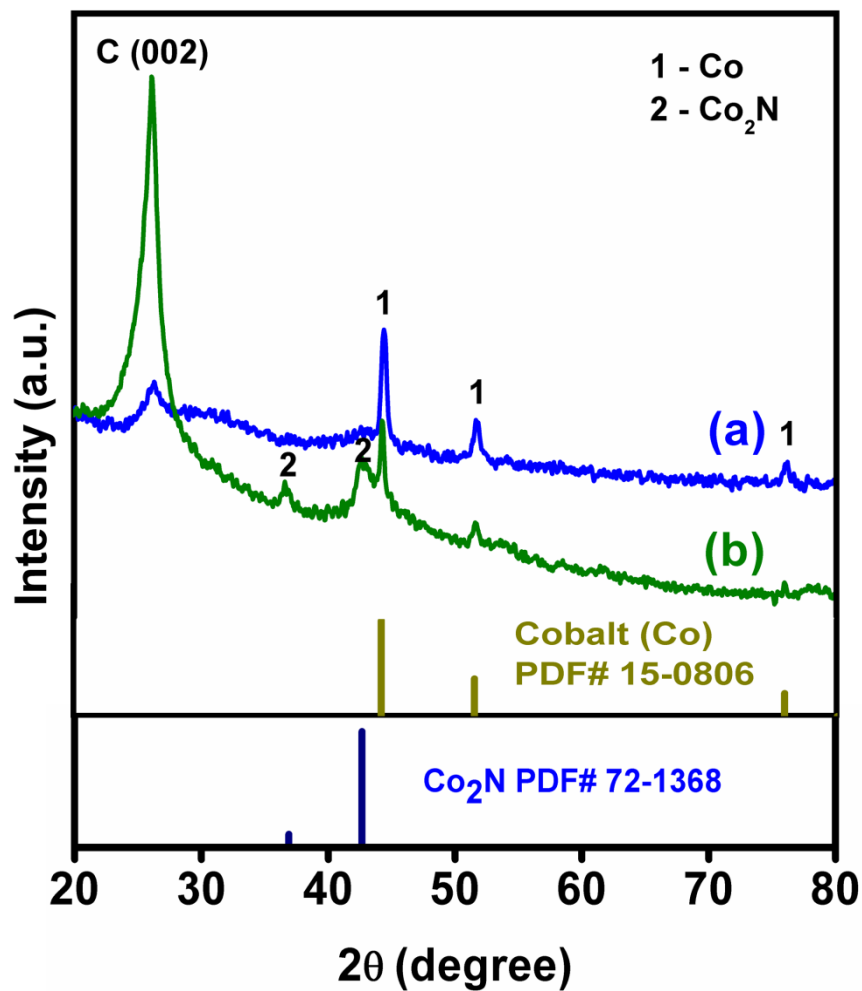


Figure 4 XRD patterns Co-N-C-1 (a) Co-N-C-2 (b)

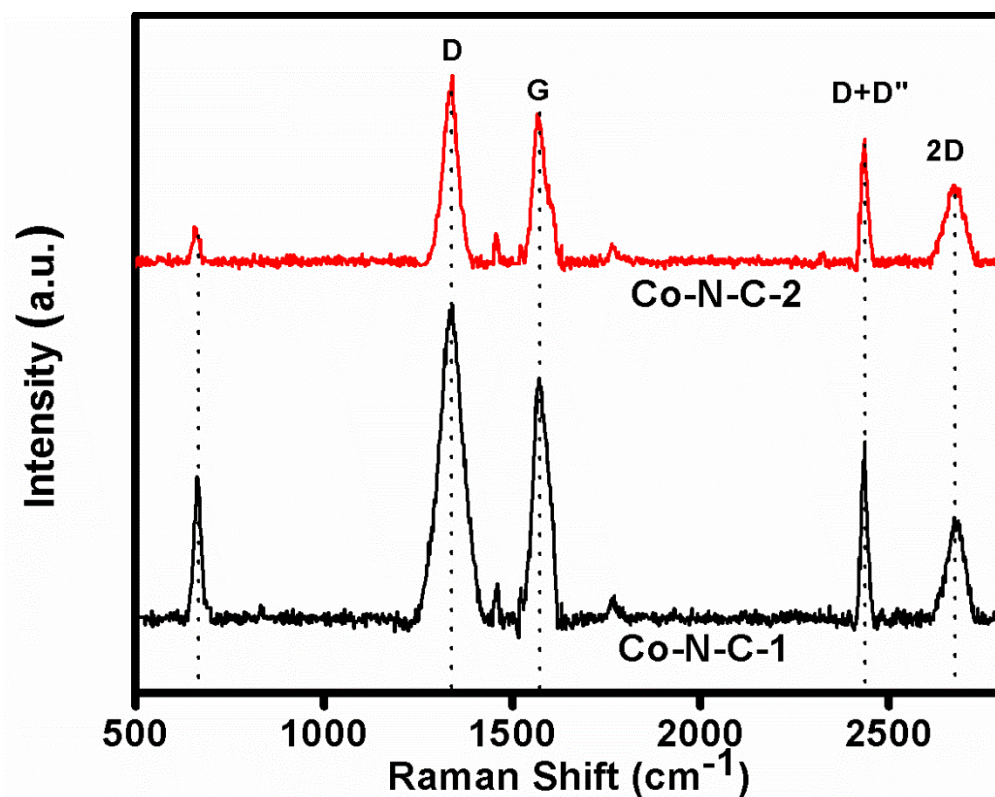


Figure 5 Raman spectrum of Co-N-C-1, Co-N-C-1-AW and Co-N-C-2

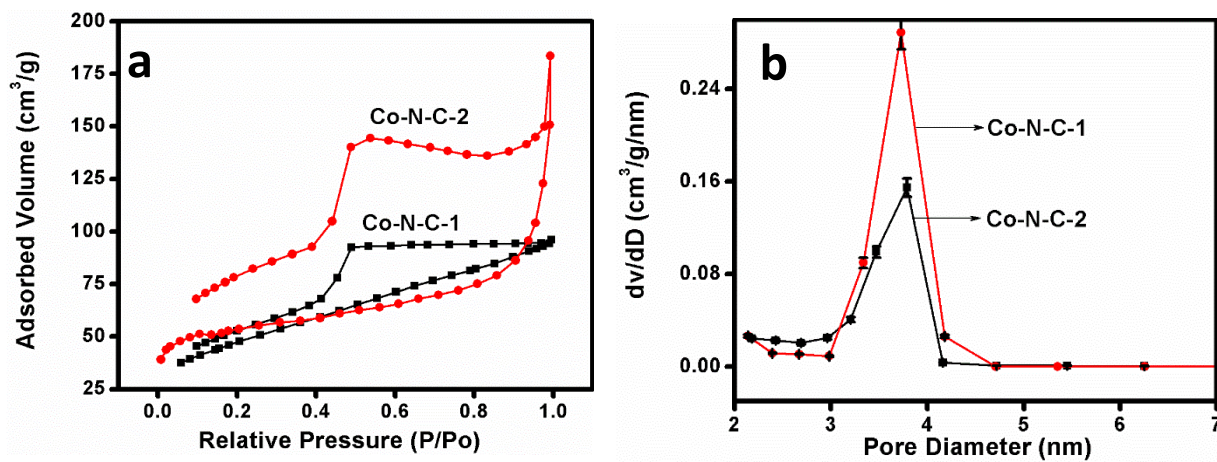


Figure 6 Nitrogen adsorption/desorption isotherm (a) and pore-size distribution curves (b) of Co-N-C-1 and Co-N-C-2.

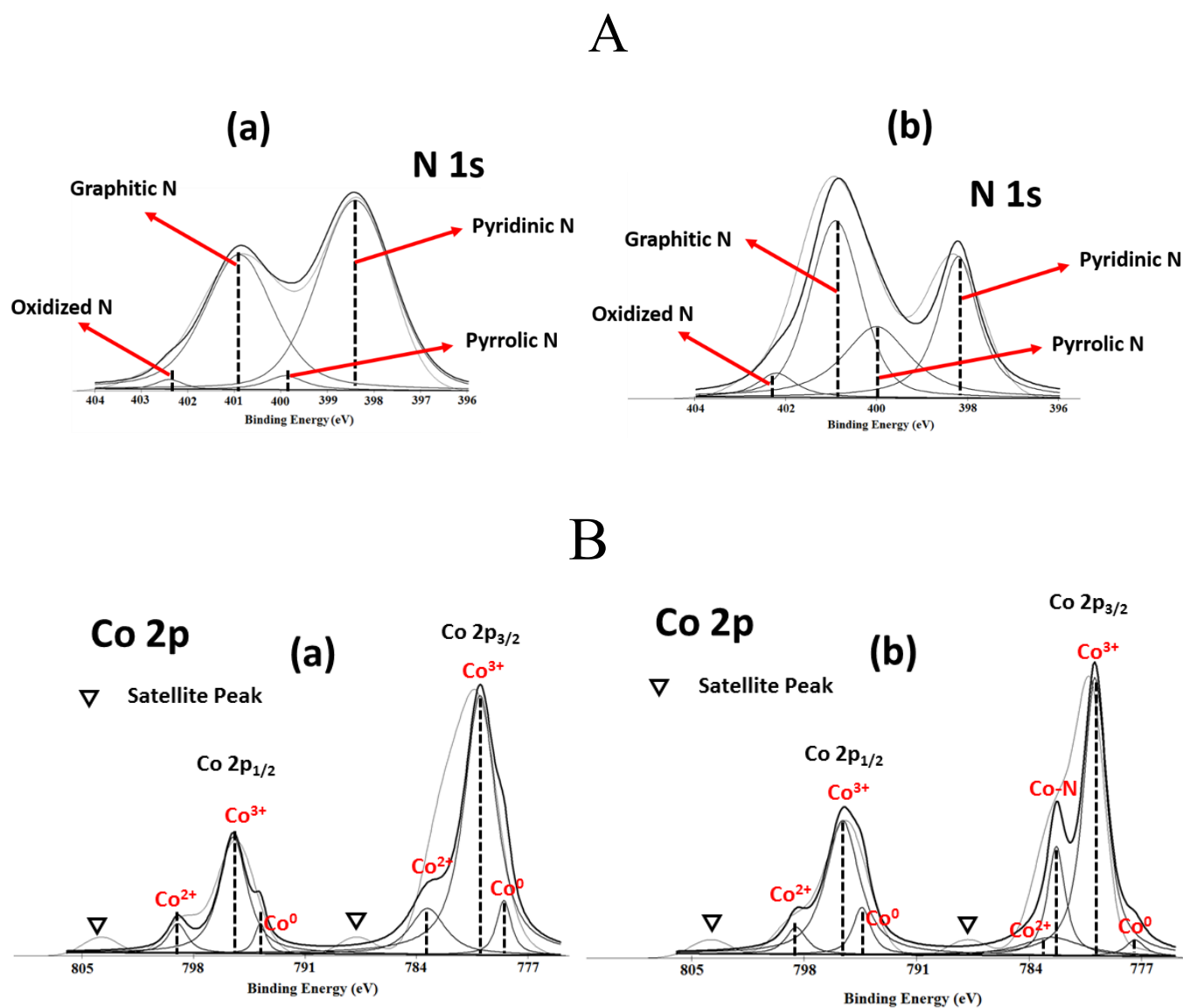


Figure 7 A: High-resolution N_{1s} XPS of Co-N-C-1 (a) Co-N-C-2 (b) ; B: High-resolution Co_{2p} XPS of Co-N-C-1 (a), Co-N-C-2 (b).

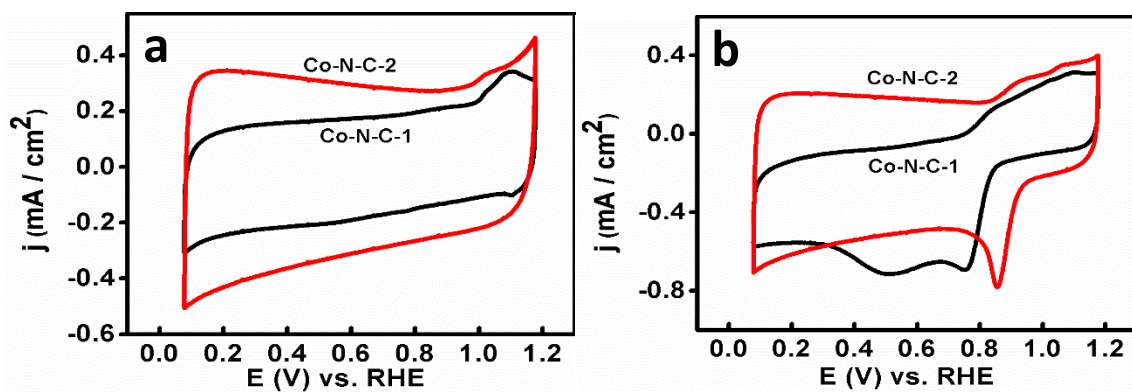


Figure 8 Overlay of CVs recorded on Co-N-C-1 and Co-N-C-2 in nitrogen (a) and oxygen (b) saturated 0.1 M KOH; Scan rate: 50 mVs⁻¹.

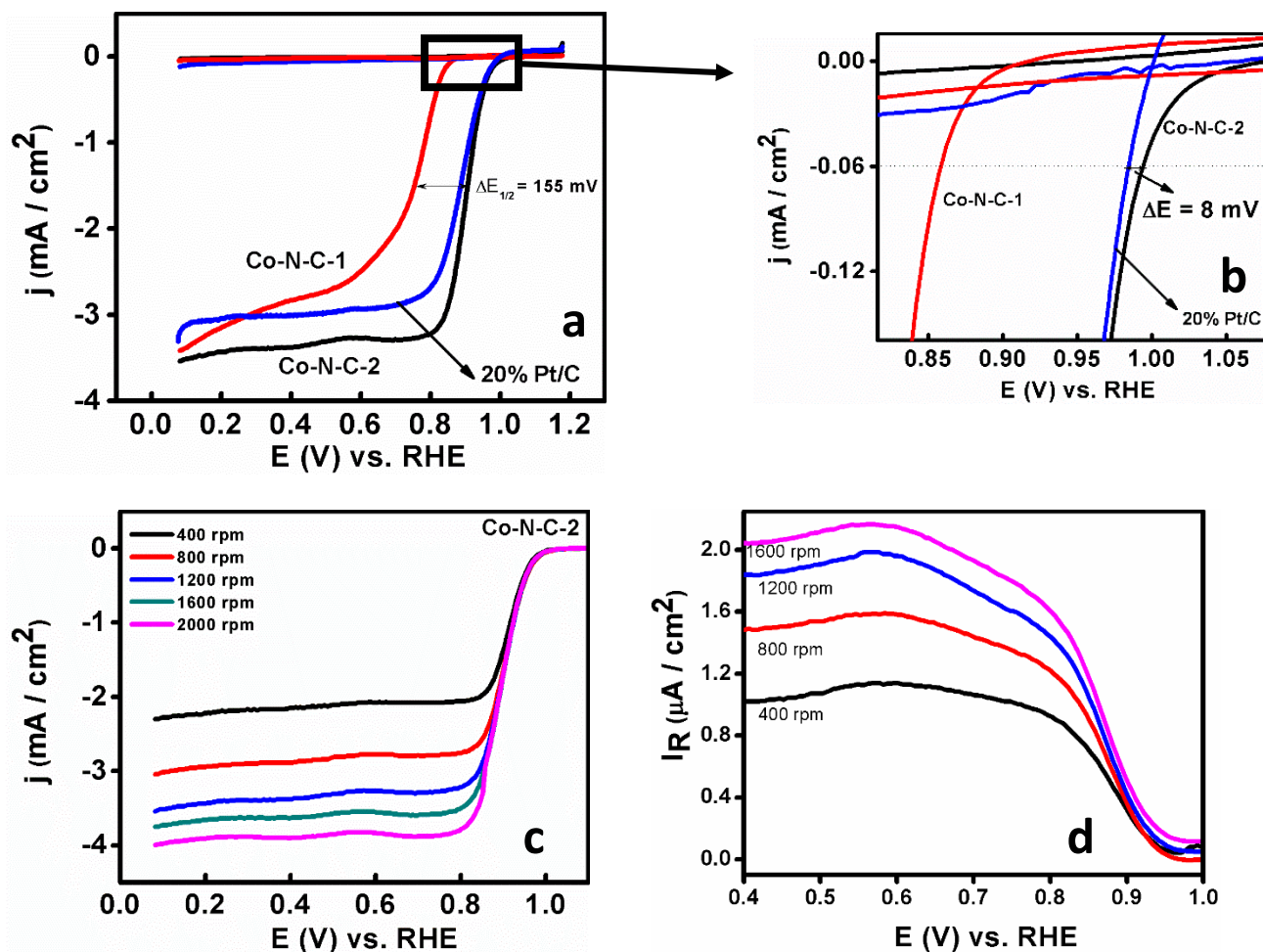


Figure 9 Polarization curves recorded using catalyst coated rotating ring disk electrode in oxygen saturated 0.1 M KOH: Comparison of Co-N-C-1 and Co-N-C-2 disk currents with 20% Pt/C (a), Enlarged view of 'a' (b), Disk currents (c) and ring currents (d) obtained from different rotation speed on Co-N-C-2; Catalyst Loading: 100 μ g/cm².

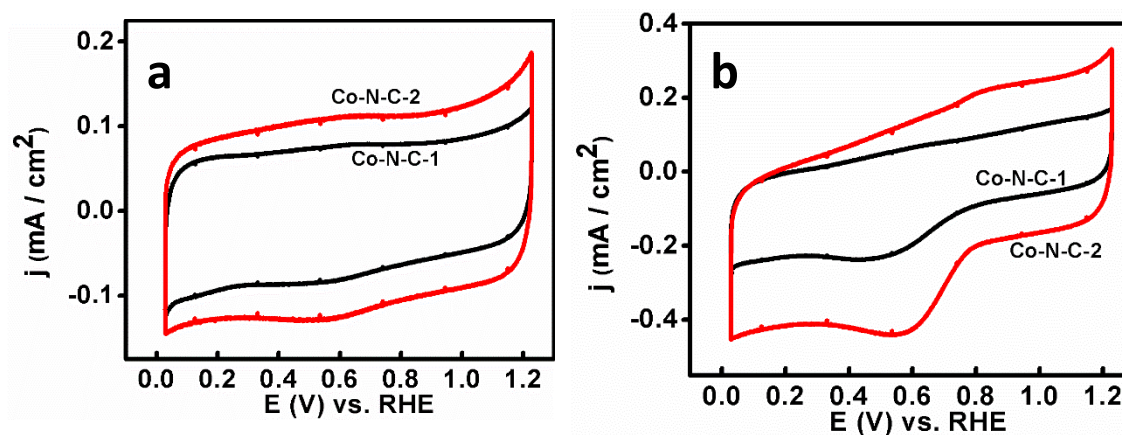


Figure 10 Overlay of CVs recorded on Co-N-C-1 and Co-N-C-2 in nitrogen (a) and oxygen (b) saturated 0.5 M H₂SO₄; Scan rate: 50 mVs⁻¹.

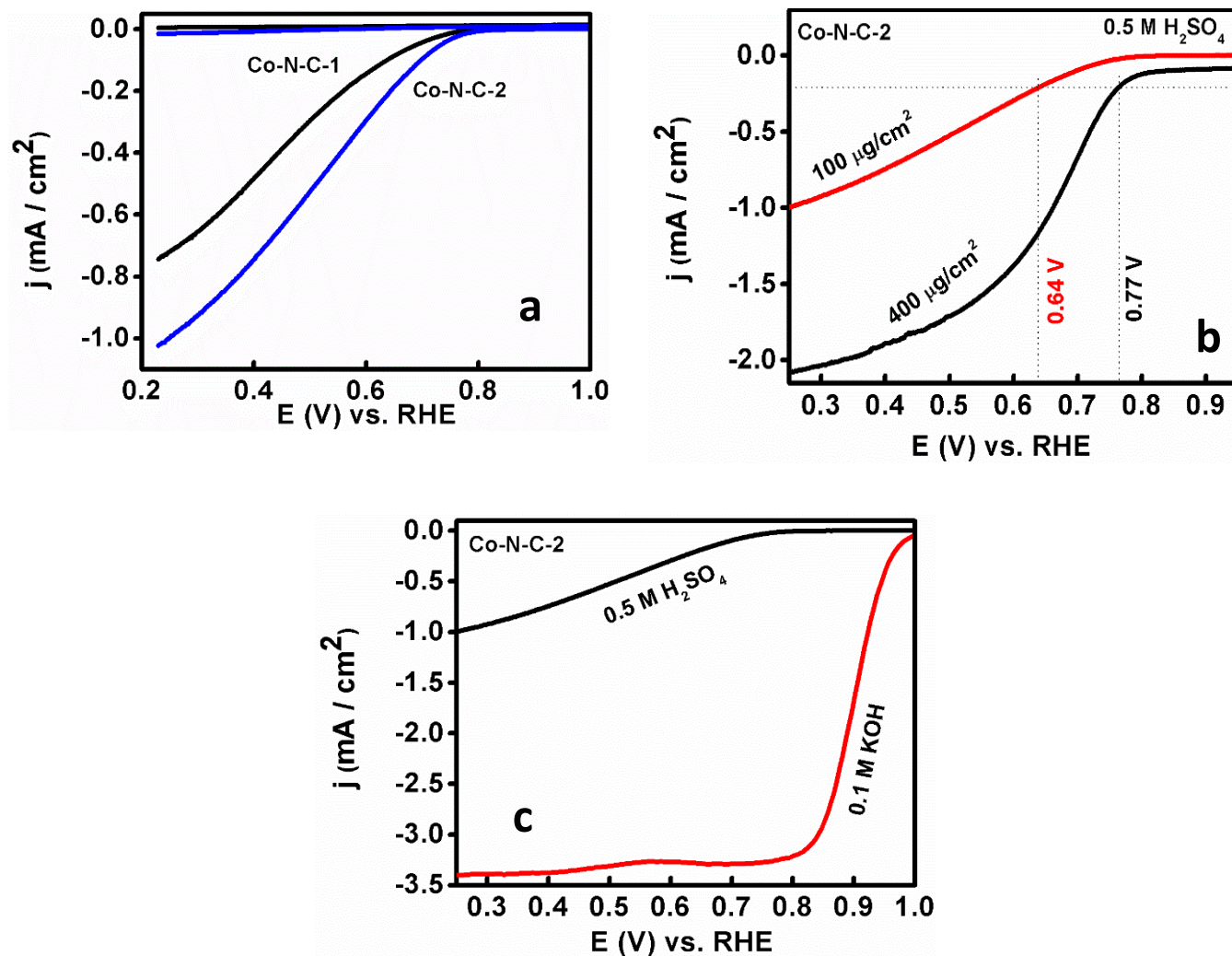


Figure 11 Polarization curves recorded using catalyst coated rotating ring disk electrode in oxygen saturated 0.5 M H₂SO₄: Comparison of Co-N-C-1 and Co-N-C-2 disk currents (a), ORR activity of different Co-N-C-2 catalyst loadings (b), Comparison of disk currents obtained at 1200 rpm in 0.1 M KOH and 0.5 M H₂SO₄.

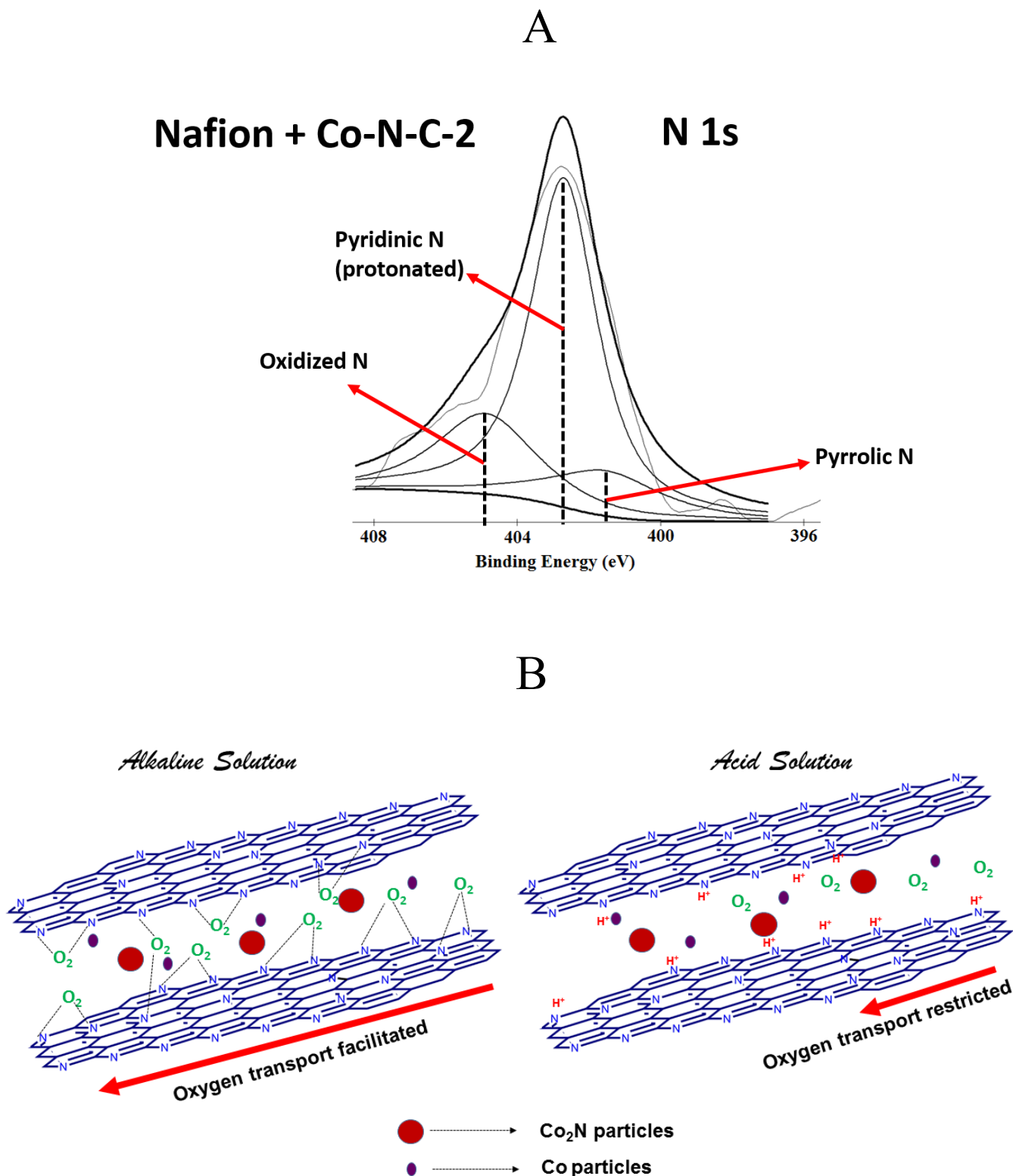


Figure 12 A: High-resolution N_{1s} XPS of Co-N-C-2-Nafion® mixture; B: Cartoon showing the oxygen transport to active sites in alkaline and acidic environments.

References

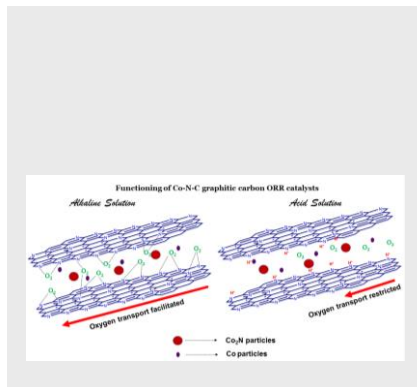
- [1] M. Shao, Q. Chang, J.-P. Dodelet, R. Chenitz, *Chem. Rev.* **2016**, *116*, 3594-3657.
- [2] C. W. B. Bezerra, L. Zhang, K. Lee, H. Liu, A. L. B. Marques, E. P. Marques, H. Wang, J. Zhang, *Electrochim. Acta* **2008**, *53*, 4937-4951.
- [3] R. Jasinski, *Nature* **1**, 1212-1213, 201, 964
- [4] K. Strickland, E. Miner, Q. Jia, U. Tylus, N. Ramaswamy, W. Liang, M.-T. Sougrati, F. Jaouen, S. Mukerjee, *Nat. Commun.* **2015**, *6*.
- [5] U. Tylus, Q. Jia, K. Strickland, N. Ramaswamy, A. Serov, P. Atanassov, S. Mukerjee, *J. Phys. Chem. C* **2014**, *118*, 8999-9008.
- [6] A. Zitolo, V. Goellner, V. Armel, M.-T. Sougrati, T. Mineva, L. Stievano, E. Fonda, F. Jaouen, *Nat. Mater.* **2015**, *14*, 937-942.
- [7] a. M. A. Abbas, J. H. Bang, *Chem. Mater.* **2015**, *27*, 7218-7235; b. Q. He, E. J. Cairns, *J. Electrochem. Soc.* **2015**, *162*, F1504-F1539.
- [8] M. Lefèvre, E. Proietti, F. Jaouen, J.-P. Dodelet, *Science* **2009**, *324*, 71-74.
- [9] V. Nallathambi, N. Leonard, R. Kothandaraman, S. C. Barton, *Electrochem. Solid-State Lett.* **2011**, *14*, B55-B58.
- [10] X. Xia, F. Zhang, X. Zhang, P. Liang, X. Huang, B. E. Logan, *ACS Appl. Mater. Interfaces* **2013**, *5*, 7862-7866.
- [11] S. Zhao, H. Yin, L. Du, L. He, K. Zhao, L. Chang, G. Yin, H. Zhao, S. Liu, Z. Tang, *ACS Nano* **2014**, *8*, 12660-12668
- [12] A. Serov, U. Tylus, K. Artyushkova, S. Mukerjee, P. Atanassov, *Appl. Catal., B* **2014**, *150-151*, 179-186.

- [13] X. Su, J. Liu, Y. Yao, Y. You, X. Zhang, C. Zhao, H. Wan, Y. Zhou, Z. Zou, *Chem. Commun. (Cambridge, U. K.)* **2015**, *51*, 16707-16709
- [14] G. Wu, K. L. More, C. M. Johnston, P. Zelenay, *Science* **2011**, *332*, 443-447.
- [15] a. L. Dai, Y. Xue, L. Qu, H.-J. Choi, J.-B. Baek, *Chem. Rev.* **2015**, *115*, 4823-4892; b. K. Sakaushi, K. Uosaki, *ChemNanoMat* **2016**, *2*, 99-103.
- [16] a. P. Song, Y. Wang, J. Pan, W. Xu, L. Zhuang, *J. Power Sources* **2015**, *300*, 279-284; b. Y. Qian, P. Du, P. Wu, C. Cai, D. F. Gervasio, *J. Phys. Chem. C* **2016**, *120*, 9884-9896.
- [17] Y. Li, W. Zhou, H. Wang, L. Xie, Y. Liang, F. Wei, J.-C. Idrobo, S. J. Pennycook, H. Dai, *Nat. Nanotechnol.* **2012**, *7*, 394-400.
- [18] N. Ramaswamy, S. Mukerjee, *Adv. Phys. Chem.* **2012**, *2012*, 17.
- [19] a. X. Zhong, L. Liu, Y. Jiang, X. Wang, L. Wang, G. Zhuang, X. Li, D. Mei, J.-g. Wang, D. S. Su, *ChemCatChem* **2015**, *7*, 1826-1832 b. X. Zhong, Y. Jiang, X. Chen, L. Wang, G. Zhuang, X. Li, J.-g. Wang, *J. Mater. Chem. A* **2016**, *4*, 10575-10584.
- [20] P. Subramanian, A. Schechter, *J. Electrochem. Soc.* **2016**, *163*, F428-F436.
- [21] S. Liu, Y. Dong, Z. Wang, H. Huang, Z. Zhao, J. Qiu, *J. Mater. Chem. A* **2015**, *3*, 19657-19661.
- [22] J. Yan, H. Meng, W. Yu, X. Yuan, W. Lin, W. Ouyang, D. Yuan, *Electrochim. Acta* **2014**, *129*, 196-202.
- [23] G.-L. Chai, Z. Hou, D.-J. Shu, T. Ikeda, K. Terakura, *J. Am. Chem. Soc.* **2014**, *136*, 13629-13640.
- [24] X. Wang, F. Zhang, X. Zhu, B. Xia, J. Chen, S. Qiu, J. Li, *J. Colloid Interface Sci.* **2009**, *337*, 272-277.
- [25] R. Narula, S. Reich, *Phys. Rev. B* **2008**, *78*, 165422.

- [26] D. H. Karweik, N. Winograd, *Inorg. Chem.* **1976**, *15*, 2336-2342.
- [27] U. I. Kramm, I. Herrmann-Geppert, P. Bogdanoff, S. Fiechter, *J. Phys. Chem. C* **2011**, *115*, 23417-23427.
- [28] G. V. Zhutaeva, V. A. Bogdanovskaya, E. S. Davydova, L. P. Kazanskii, M. R. Tarasevich, *J. Solid State Electrochem.* **2014**, *18*, 1319-1334.
- [29] F. Jaouen, A. M. Serventi, M. Lefèvre, J.-P. Dodelet, P. Bertrand, *J. Phys. Chem. C* **2007**, *111*, 5971-5976.
- [30] D. Prasai, J. C. Tuberquia, R. R. Harl, G. K. Jennings, K. I. Bolotin, *ACS Nano* **2012**, *6*, 1102-1108.
- [31] G. Zhong, H. Wang, H. Yu, H. Wang, F. Peng, *Electrochim. Acta* **2016**, *190*, 49-56.
- [32] M. Rauf, Y.-D. Zhao, Y.-C. Wang, Y.-P. Zheng, C. Chen, X.-D. Yang, Z.-Y. Zhou, S.-G. Sun, *Electrochem. Commun.* **2016**, *73*, 71-74.

FULL PAPER

New Active Site Identification: Co_2N nanoparticles evolved after post treatment steps improves the oxygen reduction activity both in alkaline and acid solution. Confinement of metallic Co_2N particles within graphitic carbon sheets protects the particles from leaching during oxygen reduction experiments in acidic solution, however protonation limits the kinetics of oxygen reduction.



*Palaniappan Subramanian, Roopathy Mohan and Alex Schechter**

Page No. – Page No.

Unraveling Oxygen Reduction Sites in Graphitic Carbon Co-N-C type Electrocatalysts Prepared from Single Precursor Pyrolysis

Accepted Manuscript